공학석사학위논문

Synthesis of Stimuli-Responsive Pt-Nanocluster Assembly against Chemoresistant Hepatocellular Carcinoma

간세포암의 약물저항성에 대응한 자극반응성 Pt 나노클러스터 조립체의 합성

2017년 2월

서울대학교 대학원

화학생물공학부 에너지환경화학융합기술전공

백승민

Abstract

Synthesis of Stimuli-Responsive Pt Nanocluster Assembly against Chemoresistant Hepatocellular Carcinoma

Seungmin Baik
Chemical Convergence for Energy and Environment
School of Chemical and Biological Engineering
The Graduate School
Seoul National University

One of the major conundrums of cancer therapy is chemoresistance. A considerable resistance of tumors to conventional chemotherapeutic agents compromises the response rate, and therefore, the overall efficacy of established medical treatments against the disease.

Small-sized platinum (Pt) nanocluster has been spotlighted as an alternative anticancer agent for its potency against cancer cells by virtue of the leached Pt ions. However, nonspecific treatment of Pt nanocluster would also incur toxicity to normal tissues, and this potential risk calls for an intricate delivery system, which would enhance the Pt nanocluster

with preferential tumor-targeting and controlled Pt activation and release.

In an effort to further the therapeutic potential of Pt nanocluster with a coordinated delivery system and to overcome the limitations of conventional chemotherapy, we synthesize a Pt-nanocluster assembly (Pt-NA) consisting of polymeric ligands with pH-sensitivity and cancer cell-targeting peptide encapsulating Pt nanoclusters. The Pt-NA is designed in such a way that it would remain latent in circulation, target the sporadic cancer cell subpopulations, release small Pt nanoclusters in acidic subcellular regions via pH-responsive dissociation, and eventually induce damage to diseased cells.

The efficacy of Pt-NA as a prospective anticancer agent is demonstrated *in vitro* and *in vivo* in hepatocellular carcinoma (HCC) model, which is often associated with the resistance to Cisplatin, a Pt-based commercial anticancer agent.

Keywords: Nanocluster, functional surface ligand, self-assembly, stimuli-responsiveness, chemoresistance, drug delivery system, cancer therapy.

Student Number: 2014-22592

Contents

List of Schemes

List of Figures

Chapter 1. Introduction

Chemoresistance is one of the major hurdles against cancer therapy. Also referred to as multidrug resistance (MDR), many cancers including breast, ovarian, lung, and liver cancers develop resistance to chemotherapy drugs as the mixed populations of malignant cells undergoing chemotherapy shift toward higher composition of drug-resistant cells.[1] The resistance of tumors to conventional chemotherapy drugs undermines the response rate of established medical treatment, and it is evident that the decreasing efficacy of medical treatment translates to higher mortality rate. Among a number of cancers associated with chemoresistance, hepatocellular carcinoma (HCC) poses a serious threat as the second leading cause of cancer-associated deaths globally[2] since this cancer is particularly notorious for its inherent resistance to conventional drugs.[3]

In an effort to solve the imposing problem of chemoresistant cancers, nanomedicine has evolved as a competent platform for the development of innovative cancer therapy.[4-7] Among a number of candidate therapeutic agents, small-sized Pt nanocluster is considered capable of overcoming the chemoresistance issue. Previous reports demonstrate that Pt nanoparticles can eradicate cancer cells[8-17] due to the free Pt ions

leaching from particles under low pH conditions including the cell endosome.[10,11] Particularly, the particle size regime down to less than 3 nm maximizes the percentage of surface Pt atoms up to more than 50%,[18,19] leaving the atoms prone to corrosion via increased oxygen adsorption and water oxidation[19] and eventually facilitating Pt ion release for therapeutic potency. Nevertheless, Pt-based compounds are highly toxic to normal tissues as well[20,21] and simple injection of Pt nanoclusters to cancer patients would only aggravate the disease with nonspecific toxicity. Targeted delivery and controlled Pt ion release profile are prerequisites for a rational treatment of cancer with the double-edged therapeutic agent of high potency and toxicity.

Self-assembled nanostructure may suggest a reliable solution to endow Pt nanoclusters with controllable functionalities,[22-24] and stimuli-responsive nanoparticle has been a frequently employed strategy not only in bio- or chemosensors *in vitro*[25-30] but also in advanced drug delivery systems *in vivo*.[31-35] We conjectured that the anticancer activity of the Pt-based nanomedicine can be harnessed by the assembly of ultrasmall Pt nanocrystals with pH-responsive encapsulating ligands.

In line with such proof of concept, we report on the design and synthesis of a Pt nanocluster assembly (Pt-NA) sensitive to low pH in tumor by encapsulating Pt nanoclusters within pH-responsive polymers and derivatizing the assembly with a HCC cell-targeting peptide.

Compared to the previously reported Pt nanoparticle-based drugs,[8-11] the Pt-NA may differentiate itself with the following advancements: Pt-NA remains inactive in peripheral blood during circulation until the cancer-cell targeting peptide guides the assembly to tumor subpopulation; pH-responsive functional group in polymer ligand protonated in an acidic intracellular environment triggers the dissociation of the structure bursting out Pt nanoclusters; the exposed Pt nanoclusters thanks to their large specific surface area accelerate the release of free Pt ions, an active therapeutic agent, inside the tumor cells for an effective cancer treatment.

Our overarching design and therapeutic strategy of Pt-NA are schematically illustrated (**Scheme 1**). We hypothesize that the intravenously injected Pt-NA accumulates in HCC lesion via the enhanced permeability and retention (EPR) effect[36,37] and SP94 specific ligands facilitate receptor-mediated endocytosis into HCC cells.[38] Following the endocytosis, the pH-sensitive ligand capsule at Pt-NA exposed to endolysosomal acidification[39-41] is disrupted. Pt nanoclusters exposed to low pH subcellular environment exude free Pt ions in HCC cells, and the cancer cells are eradicated because of the active targeting strategy.

Chapter 2. Experimental Section

2.1. Chemicals

Platinum (II) acetylacetonate, oleylamine, oleic acid, 1-octadecene, superhydride solution, β-benzyl-L-aspartate N-carboxy anhydride (BLA-NCA), 1-(3-aminopropyl)imidazole (API), Pluronic® F-127, 6-maleimidohexanoic acid (MA), rhodamine B isothiocyanate (RITC), dicyclohexylcarbodiimide (DCC), 4-dimethylaminopyridine (DMAP), and N,N-dimethylformamide were purchased from *Sigma-Aldrich*. 1,2-distearoyl–*sn*-glycero-3-phosphoethanolamine-N-[methoxy(poly ethylene glycol)-2000] (ammonium salt) (DSPE-mPEG(2000)) was purchased from *Avanti Polar Lipids, Inc.* Solvents including ethanol, hexane, dichloromethane (DCM), tetrahydrofuran, (THF), and dimethyl sulfoxide (DMSO) were purchased from *Samchun*. Biological media including phosphate buffered saline (PBS) were purchased from *Gibco*. All the reagents were used as received from commercial sources and without any further purification steps.

2.2. Preparation of Pt Nanocluster Assembly (Pt-NA)

Synthesis of Pt Nanoclusters

Ultrasmall-sized Pt nanoclusters are synthesized via heat-up method in which the platinum precursor of $Pt(acac)_2$ is thermally decomposed within the mixed solutions of oleylamine and oleic acid. Firstly, $Pt(acac)_2$ (0.16g), oleylamine (14 ml), and oleic acid (0.12 ml) were mixed in an 100 ml round bottom flask, and the mixture was heated to 70 °C with vigorous stirring and under vacuum for 1 hour. After the degassing, the solution was heated up to 170 °C at 3 °C per minute. superhydride solution (0.4 ml) was injected into the reaction mixture, and the mixture was aged at 170 °C for 10 minutes. The resulting Pt nanoclusters were washed with ethanol and hexane in order to remove excess reactant, and the nanoclusters were re-dispersed in hexane for further experiment.

pH-Sensitive Peptide Ligand (Octadecylamine-p(API-Asp)$_{10}$)

Synthesis of octadecylamine-p(API-Asp)$_{10}$ was conducted according to our previously reported methods.[42] Firstly, octadecylamine (0.3 g, 1.2 mmol) and BLA-NCA (3 g, 12 mmol) were heated at 40 °C in a mixture containing dimethylformamide (DMF; 20 ml) and CH_2Cl_2 (50 ml) for 2 days. After rotary evaporation to remove CH_2Cl_2, the resulting octadecylamine-p(Bz-ASP)$_{10}$ was precipitated in diethyl ether, and isolated via centrifugation at 3500 rpm (5 min). Then, pH-sensitive octadecylamine-p(API-Asp)$_{10}$ was synthesized via aminolysis of the

octadecylamine-p(Bz-ASP)$_{10}$ with API. Octadecylamine-p(Bz-Asp)$_{10}$ (0.2 g, 74.8 μmol) was dissolved in anhydrous DMF (5 ml), followed by reaction with API (1 g, 7.9 mmol) under N_2 gas at 25 °C and stirred for 12 h. The reaction mixture was added dropwise into a cooled aqueous solution of 0.1 N HCl (20 ml) and dialyzed against a 0.01 N HCl solution three times (Spectra/Por; MWCO: 1,000 Da) for 24 h. Lyophilization of the solution yielded octadecylamine-p(API-Asp)$_{10}$ and the final product was verified by proton nuclear magnetic resonance (^{1}H-NMR) spectroscopy. ^{1}H-NMR spectra were recorded in DMSO-d6 at room temperature using a Bruker NMR Spectrometer (Bruker, Germany) at 500 MHz.

^{1}H-NMR (500 MHz, DMSO-d6) for octadecylamine–p(API-Asp)$_{10}$: δ = 7.8 ppm (1H, s, −NCH═N– of imidazole ring), 7.7 ppm (1H, s, −NCH═CH– of imidazole ring), 7.3 ppm (1H, s, −CH═CH–N– of imidazole ring), 4.5 ppm (1H, m, –NHCHC═O−), 4.0 ppm (2H, s, ═NCH2CH2), 3.0 ppm (2H, s, −NHCH2CH2−), 2.6 ppm (2H, m, −CH2C═ONH−), 1.8 ppm (2H, s, −CH2CH2CH2−), 1.2 ppm (17H, s, −CH2– of octadecylamine), and 0.8 ppm (3H, t, CH3– of octadecylamine).

6-Maleimidohexanoic Acid-Pluronic F127 (MA-F127) Conjugates

Pluronic F127 powder (1 g, 0.08 mmol) was dissolved in anhydrous THF (5 ml). 6-maleimidohexanoic acid (MA; 66 mg, 0.3 mmol), dicyclohexylcarbodiimide (DCC; 98 mg, 0.5 mmol), and 4-dimethylaminopyridine (DMAP; 57 mg, 0.5 mmol) were sequentially added to the solution. The reaction mixture was stirred for 24 h in order to conjugate Pluronic F127 with MA, and the product was precipitated in diethyl ether and dried under vacuum. MA-F127 conjugate was confirmed via ^{1}H-NMR (Figure S5).

^{1}H-NMR (500 MHz, DMSO-d6) for MA-F127 conjugate (Figure S5): δ = 7.0 ppm (1H, s, −CH═CH-C═O of MA), 3.4–3.6 ppm (848H, m, −CH2CH2O– of Pluronic F127), and 1.0 ppm (210H, d, −CH2CH–(CH3)O– of Pluronic F127).

Preparation of the pH-Sensitive Pt-NA

Octadecylamine–p(API-Asp)$_{10}$ (20 mg) in methanol (0.2 ml) was introduced dropwise into the mixture of Pt nanoclusters (1.2 mg) and MA–F127 (10 mg) in $CHCl_3$ (3 ml). After stirring, the mixture was dried via rotary evaporation. Phosphate-buffered saline (PBS; pH 7.4, 4 ml) was added to re-disperse the mixture. The mixture was ultrasonicated for 30 min with a benchtop sonicator and stirred at 60°C for 6 h. The product Pt-NA was purified by centrifugation at 15,000 rpm (4 C°, 15 min) and washed with PBS buffer (150 mM, pH 7.4) to remove excess reagents.

2.3 Characterization

Transmission electron microscopy (TEM) images were obtained by a JEOL JEM-2010 electron microscope at an accelerating voltage of 200 kV. The powder X-ray diffraction (XRD) patterns were obtained by a Rigaku D/Max-3C diffractometer with Cu Kα radiation. The elemental analysis was performed by inductively coupled plasma atomic emission spectroscopy (ICP-AES) via an ICPS-7500 spectrometer (Shimadzu).

2.4 *In vitro* Studies

Pt Ions Release Profile

The Pt ions release profile was obtained using dialysis tubes (Float-A-LyzerR; cutoff 0.1-0.5 kDa, SpectrumR Laboratories, Inc., USA) at 37 °C. In a typical experiment, Pt nanoclusters were encapsulated by DSPE-mPEG(2000) for phase transfer to aqueous media. The PEGylated Pt nanoclusters (5 mg ml^{-1}) in deionized water (1 ml) were placed in a dialysis tube and dialyzed against the pH-adjusted PBS (10 ml, pH 7.4, 6.8, 5.5, 5.0) with shaking at 200 rpm. The release medium was harvested at designated time interval, and the release container was replenished with fresh medium. The amount of Pt released was measured using inductively coupled plasma mass spectrometry (ICP-MS, Perkin Elmer, Waltham, MA, USA).

Particle Size Measurement of Pt-NA at Different pH

The hydrodynamic size of Pt-NA (1 mg ml^{-1}) at different pH was determined by dynamic light scattering (DLS, Zetasizer Nano ZS, Malvern Instruments Ltd., UK).

Cell Viability Test

The cell viability was determined by 3-(4,5-dimethylthiazol-2-yl)-5-(3-carboxymethoxyphenyl)-2-(4-sulphophenyl)-2H-tetrazolium (MTS) assay using the CellTiter 96 AQueous One Solution Cell Proliferation Assay kit (Promega). In a 96-well plate, the cells were seeded at a density of ~5×10^3 cells per well. After 24 hours, the cells were replenished with the fresh medium containing Pt-NA, cisplatin or vehicle at designated concentrations. After 48 hours, the culture medium was replaced by the fresh medium containing MTS (20 μl). Following 2 hours of incubation, the absorbance at 490 nm was measured by Wallac Victor 1420 Multilabel plate reader. Each experiment was triplicated.

Cellular Uptake Assay

The sorted SP+CD24+ HCCLM3 cells or MIHA cells were seeded in an 8-well cover-glass chamber (LAB-TEK, Nagle Nunc, IL, USA). The cells were treated with Pt-NA and incubated for 24 hours. Cellular uptake of the Pt-NA was observed via Nikon live-cell imaging system (Nikon). Intracellular distribution of the Pt-NA were also assessed using CLSM (Carl Zeiss). The nucleus was counterstained by the Hoechst 33342.

2.5 *In vivo* Studies

In vivo Tumorigenicity and Treatment Assay

In vivo experiments conducted with mice received an approval by the SingHealth Institutional Animal Care and Use Committee (IACUC). SP−CD24− or SP+CD24+ HCCLM3 and PLC/PRF/5-Cis cells were sorted and injected into NOD/SCID mice subcutaneously. Grown subcutaneous tumors were collected and sorted by size. Tumors of a similar size were transplanted onto the livers of mice to induce the orthotopic xenograft model. Once the orthotopic xenograft tumors were established from sorted SP+CD24+ luciferase-expressing HCCLM3 cells, the mice with a similar intensity of bioluminescence were divided into groups (6 mice per group) and administered with cisplatin (2 mg kg^{-1}), Pt-NA (2 mg kg^{-1}), sorafenib (30 mg kg^{-1}) or vehicle either intravenously by tail vein injection or orally (for sorafenib). The drugs were administered twice per week, except for sorafenib which was administered every day. The therapeutic efficacy was determined by mouse survival, and tumor volume was assessed by bioluminescence imaging from the Xenogen IVIS Lumina system after luciferin administration.

Survival and Statistical Analysis

The experimental data are presented as the mean ± standard deviation. The survival curves were derived using the Kaplan-Meier method and were statistically compared using a log-rank test. Other statistical comparisons were performed using analysis of variance or a two-tailed Student's t-test in GraphPad Prism 5 software. Differences were considered statistically significant when the P-values were less than 0.05.

Chapter 3. Results and Discussion

3.1. Design and Synthesis of Pt-Nanocluster Assembly

The Pt-NA consists of the following components: ultrasmall Pt nanoclusters and two polymeric ligands of octadecylamine-p(API-Asp)$_{10}$ and MA-F127 conjugate. This section involves a detailed discussion on the following steps: synthesis of Pt nanoclusters, synthesis and function of polymeric ligands, and characterization of physicochemical properties of the as-synthesized Pt-NA.

3.1.1. Ultrasmall Pt Nanoclusters

Ultrasmall Pt nanoclusters are synthesized by the thermal-decomposition of Pt(acac)$_2$, and the obtained nanoparticles have an average size of 2.5 nm and the X-ray diffraction peaks consistent with putative Pt peaks as characterized by TEM images and XRD patterns (**Figure 1, 2**). Composition and ratio of surfactant and solvent are key to the precise control of uniform size distribution. The nanoclusters of the qualifying size regime at < 3 nm as well as the uniform distribution are produced when oleylamine and oleic acid are both added as 100 equiv and 1 equiv to Pt(acac)$_2$ (**Figure 1a, b**); for oleylamine alone, addition of 1 equiv would only yield worm-shaped particles (**Figure 1c**) whereas

100 equiv added facilitates production of the nanoclusters meeting the size criteria at the expense of less uniformity (**Figure 1d**); for oleic acid alone, addition of 1 equiv resulted in a similar trend of producing worm-like nanoparticles (**Figure 1e**) but even 100 equiv did not yield the particle but rather the particles aggregated (**Figure 1f**).

The rationale behind the significance of size is as follows: the smaller the nanoparticles are, the larger the overall surface area. Subsequently, an increase in surface area facilitates the leaching of surface Pt ions in an acidic aqueous solution.[43,44] In order to confirm the size dependence of Pt leaching, two Pt nanoclusters of different average sizes at 3 nm and 10 nm are PEGylated and dialyzed against pH-adjusted PBS. Cumulative Pt ion release profile quantified by ICP-MS reveals that a greater amount of Pt ion releases from 3 nm-sized nanoclusters than from 10 nm-sized counterpart for all pH conditions, and the size-dependence holds even at pH 7.4 where the size alone shows two-fold increase in Pt ion release (**Figure 3**).

3.1.2. Functional Polymeric Ligands

Two polymeric ligands of distinct functionality are rationally designed so that the ligands may be responsive to the acidic condition within tumor microenvironment, and be able to accommodate an active targeting moiety specific to cancerous cells. Firstly, maleimide-functionalized

Pluronic F127 (MA-F127) is designed to serve as the building block of assembly structure. Maleimide group incorporated at the terminus of polymeric ligand confers the flexibility of conjugating a cancer-targeting moiety with the maleimide. Also conceived is a synthetic pH-sensitive polypeptide composed of aspartic acid (10-mer) modified with ionizable imidazole side chains and an octadecylamine tail (**Scheme 2**). Octadecylamine-p(API-Asp)$_{10}$ was synthesized based on our previously reported method.[42] Incorporation of imidazole group gives the ligand a pH sensitivity, in which the imidazole group is de-/protonated depending on the pH level of local vicinity. The de-/protonation affects the surface charge, and contributes to the disruption of assembly structure due to electrostatic repulsion. Conjugation of MA with Pluronic F127 was confirmed by ^{1}H-NMR spectrum in DMSO-d$_6$ (**Figure 4**).

3.1.3. Properties of Pt-NA

The assembly is performed by the dual solvent-exchange method with some modification[34]. The ligands are designed in such a way that maleimide groups from MA-F127 are exposed on the surface of the self-assembled structure, which can be conjugated readily with the thiol group (–SH) of any targeting peptide such as the HCC cell-specific peptide ligand SP9443 (H2N-SFSIIHTPILPLGGC-COOH)[45,46] (as schematically illustrated in **Scheme 1**).

The size of the overall self-assembled Pt-NA is ~ 100 nm as visualized by TEM images (**Figure 5a, b**) and the assembly structure with the hydrodynamic size of ~ 180 nm remains intact as determined by DLS at neutral pH of 7.4 (**Figure 6**). However, as the pH drops to ~6.0, the self-assemble structure is disrupted. The ruptured Pt-NA was demonstrated by TEM image (**Figure 5c**) and also confirmed by a sharp drop in hydrodynamic size at pH ~6.0 (**Figure 6**).

The responsiveness of Pt-NA to the tumor intracellular pH environment translates to the pH-dependence of Pt ion leaching profile for the complete Pt-NA structure. Pt-NA, structurally stable and latent at pH ~7.4, does not exhibit a significant level of leached Pt ions; at pH <6, dissociation of Pt-NA triggers acceleration of Pt ion release (**Figure 7**).

3.2. *In vitro* Efficacy and Cellular Uptake of Pt-NA

The effect of Pt-NA against chemoresistant subpopulation of HCC cells was explored *in vitro*, and compared to that of cisplatin (**Figure 8**). Against the drug-resistant SP+CD24+ cells with induced resistance towards cisplatin, Pt-NA exhibits a dose-dependent anticancer efficacy whereas cisplatin shows a negligible effect even at high dose (**Figure 8a, b**). For normal liver cell line of MIHA, the trend reverses. (**Figure 8c**) The latency of Pt-NA towards normal tissue is demonstrated *in vitro*, whereas cisplatin is highly toxic to normal cell lines.

Cellular uptake efficiency of cisplatin and Pt-NA is also examined in the drug-resistant SP+CD24+ and normal MIHA cell lines. While the amount of Pt taken up by SP+CD24+ cells is much less than that of MIHA cells for cisplatin, Pt-NA is rather taken up preferentially by the drug-resistant cells the cellular expression (**Figure 9**). Combined with much lower toxicity towards normal cell lines, Pt-NA proves its efficacy *in vitro*.

3.3. *In vivo* Therapeutic Effect and Distribution of Pt-NA

Active tumor targeting capability of Pt-NA, empowered by SP94 peptide conjugated to MA-F127, is demonstrated in vivo using an HCC orthotopic mouse model (**Figure 10**). As depicted by IVIS image, the biodistribution result of Pt-NA is quite similar to that of other nanomaterial-based anticancer agents, which accumulate mainly in liver and spleen.

Anti-HCC study accentuates the superior therapeutic efficacy of Pt-NA compared to cisplatin and sorafenib, both of which are at commercial level. The therapeutic efficacy quantified by bioluminescence signal clearly demonstrates that Pt-NA outperforms the conventional anticancer drugs. (**Figure 11a, b**) The Pt-NA-treated mice also show the highest survival rate at ~60% after 3 months (**Figure 11c**).

Chapter 4. Conclusion

In summary, a novel Pt nanocluster assembly (Pt-NA) in order to overcome chemoresistance of HCC cells was successfully synthesized. The ultrasmall size as well as uniform distribution endowed the Pt nanoclusters with high percentage of surface-leached Pt ions as a potent drug, and incorporation of rationally designed surface ligands with pH sensitivity and HCC targeting moiety augmented the overall therapeutic value of this newly introduced nanomaterial drug delivery system.

The material of Pt-NA was carefully characterized, and especially Pt ions leaching profile was thoroughly scrutinized in order to ensure that the nanoparticle size and pH serve as significant parameters for the application of Pt-based materials as anticancer agents.

Therapeutic efficacy was doubly corroborated *in vitro* and *in vivo*. Cellular uptake study and viability test, combined together, showed that Pt-NA not only delivers to cancerous cells at a great efficiency thanks to the active targeting moiety, but also remains latent and innocuous to normal cells. Pt-NA is also competent in mice model of HCC in which the Pt-ion based therapy outperforms two commercial anticancer drugs of sorafenib and cisplatin. We expect that nanomedicine, with rational design and careful study, can serve as a strong platform to tackle the limitations in cancer therapy.

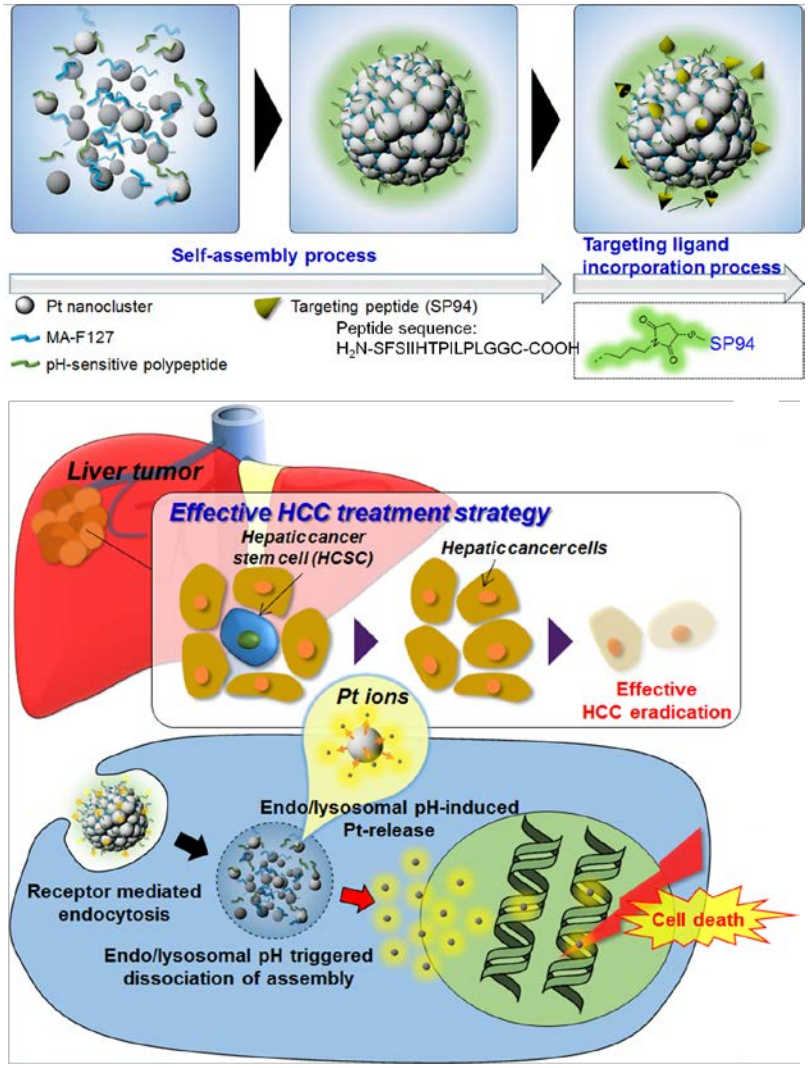

Scheme 1. Pt nanocluster assembly (Pt-NA) for a stimuli-responsive targeted therapy against chemotherapeutic resistance of hepatocellular carcinoma (HCC).

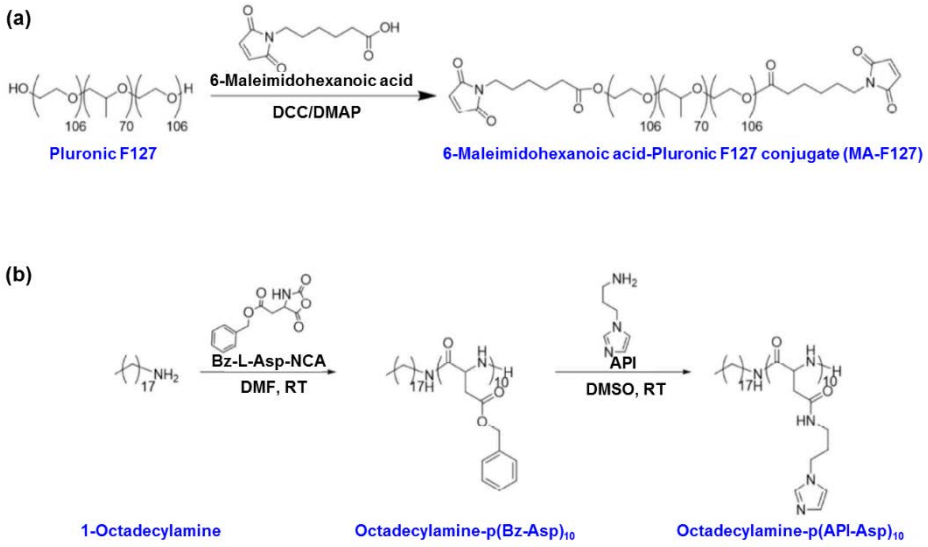

Scheme 2. Synthetic scheme of two polymeric ligands for Pt nanocluster assembly.

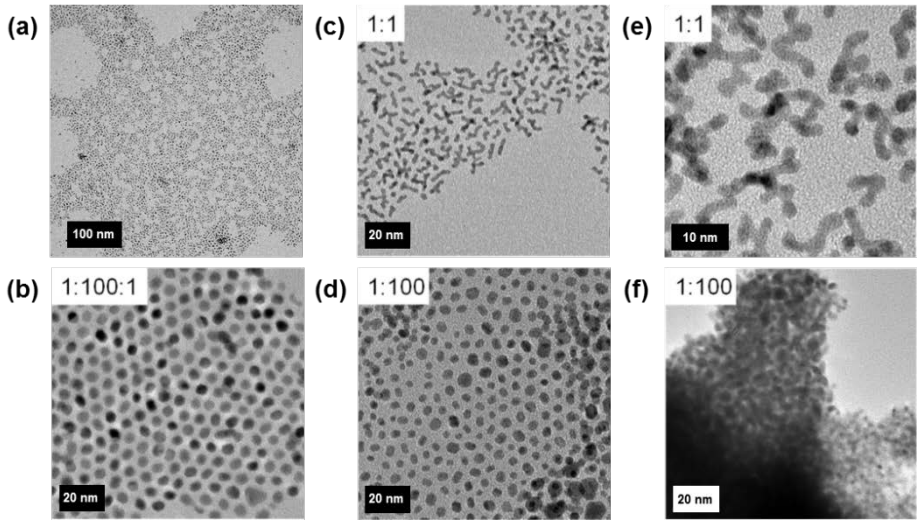

Figure 1. TEM images of Pt nanocrystals synthesized with different ratio and composition of surface capping ligands. (a, b) Pt(acac)2: oleylamine: oleic acid = 1: 100: 1. (c) Pt(acac)2: oleylamine = 1: 1. (d) Pt(acac)2: oleylamine = 1: 100. (e) Pt(acac)2: oleic acid = 1: 1. (f) Pt(acac)2: oleic acid = 1: 100.

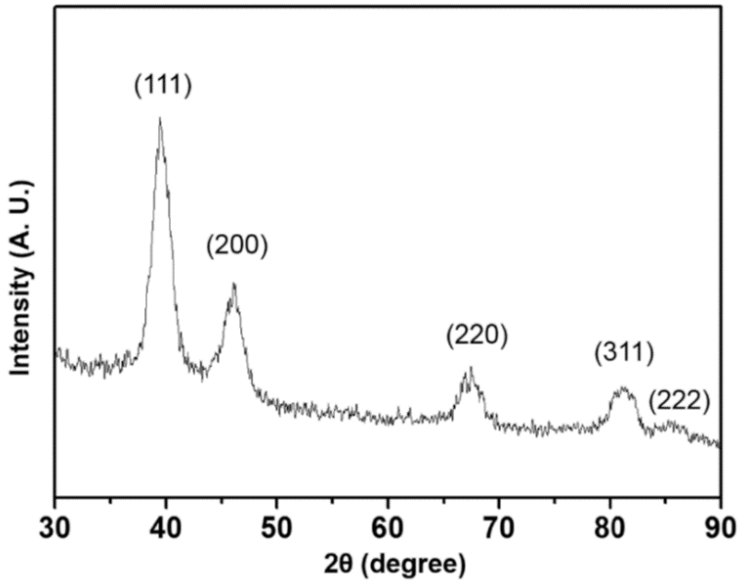

Figure 2. XRD pattern of Pt nanoclusters.

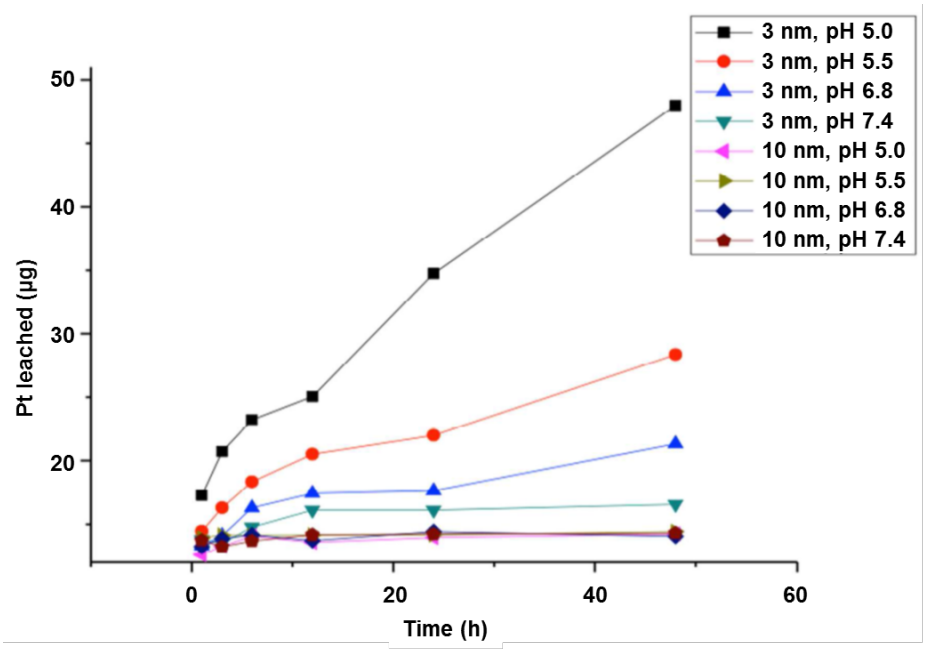

Figure 3. *In vitro* cumulative Pt ion release from Pt nanoclusters with particle size 3 nm and 10 nm at different pH (pH 7.4, 6.8, 5.5 and 5.0, Pt sample 5 mg ml^{-1}).

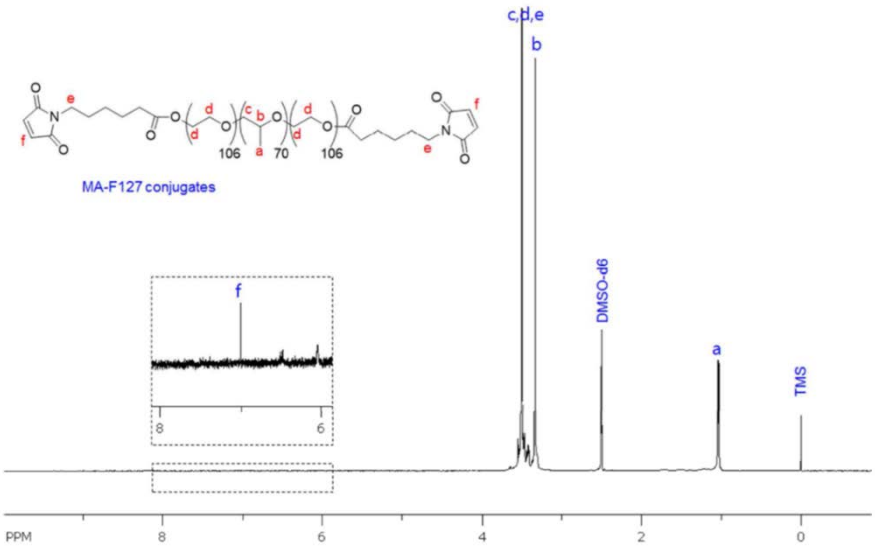

Figure 4. ^{1}H-NMR spectrum of MA-F127 conjugates in DMSO-d_6.

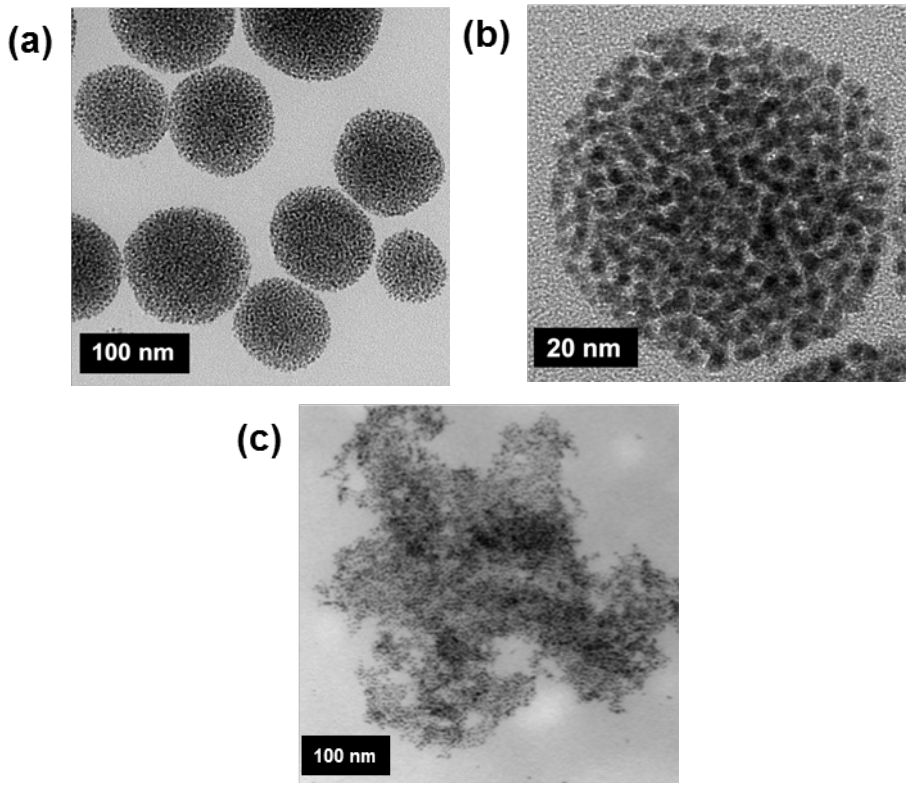

Figure 5. (a) TEM image of Pt-NA. (b) High-resolution TEM image of Pt-NA. (c) TEM image of Pt-NA dissociated at pH 6.0.

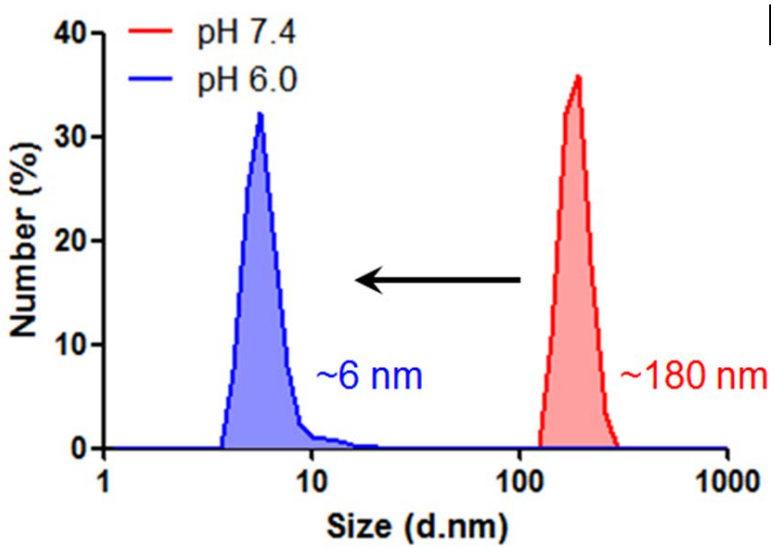

Figure 6. DLS measurement of Pt-NA as a function of pH.

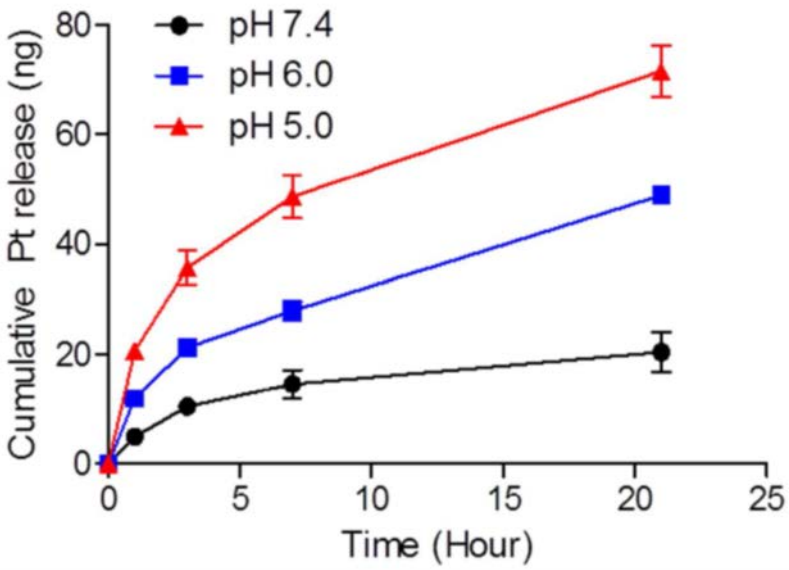

Figure 7. *In vitro* cumulative Pt ions release from Pt-NA at different pH (pH 7.4, 6.0 and 5.0, Pt sample 20 μg ml^{-1})

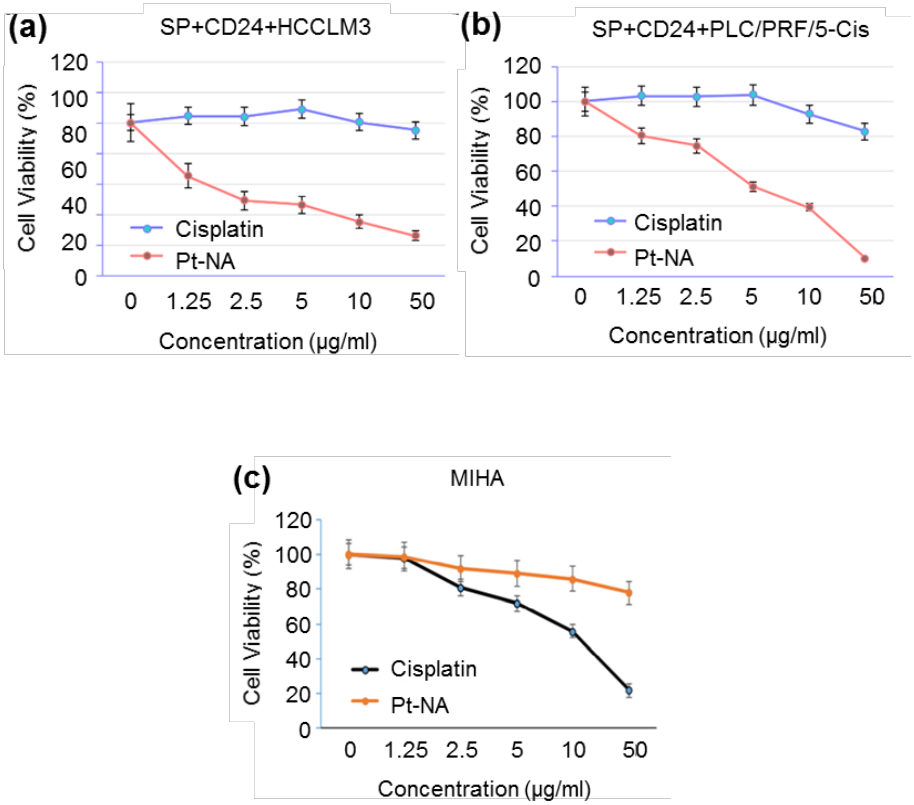

Figure 8. (a, b) Dose-dependent inhibition effects of Pt-NA and cisplatin on cell growth in the cisplatin-resistant (a) HCCLM3 and (b) PLC/PRF/5-Cis cell lines. (c) Dose-dependent inhibition effects of Pt-NA and cisplatin on cell growth in the cisplatin-resistant normal liver cell line MIHA.

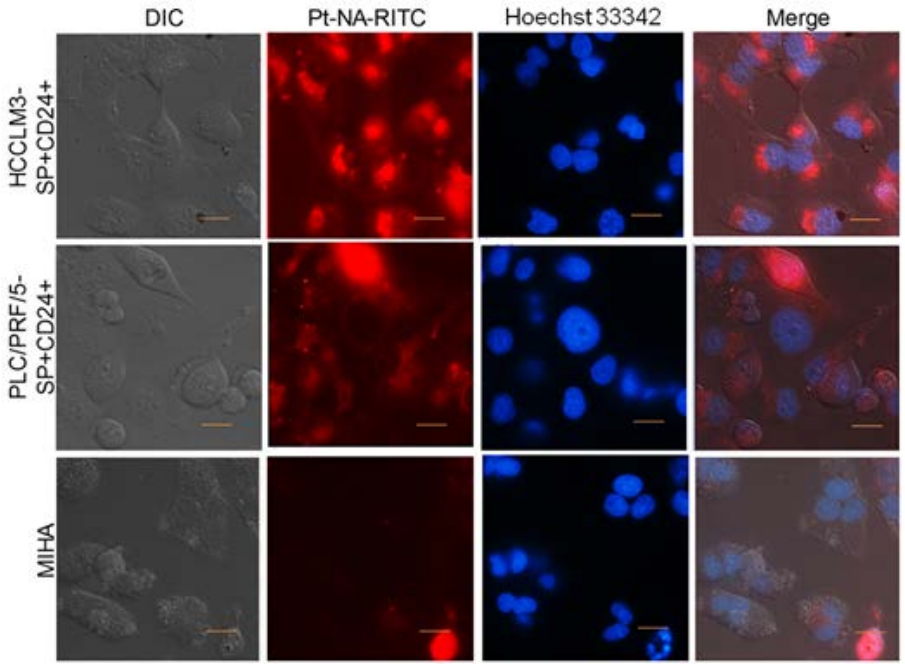

Figure 9. Cellular uptake of Pt-NA in cisplatin-resistant and cancer stem-like SP+CD24+ cells. Pt-NA uptake is minimal in the normal liver cell line MIHA (scale bar, 50 μm).

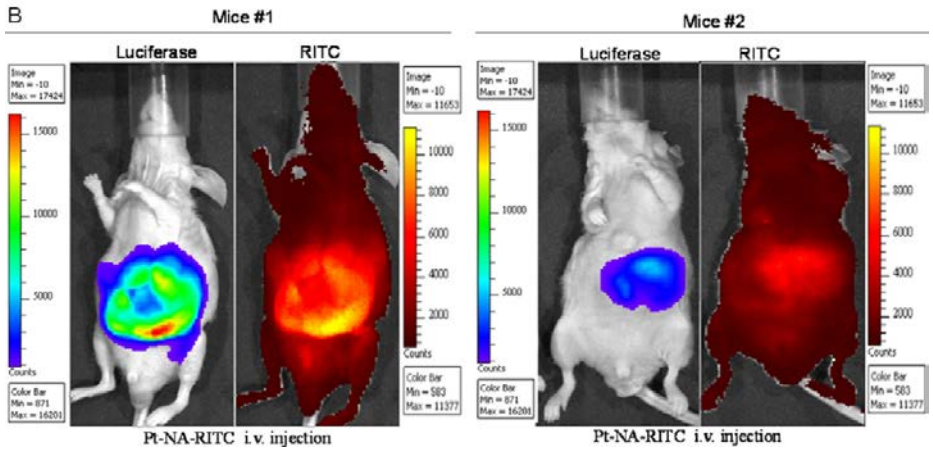

Figure 10. *In vivo* biodistribution of Pt-NA in SP+CD24+ HCCLM3 cells of representative orthotopic HCC mice with different tumor sizes (2 h after injection, tumors are established from different number of sorted SP+CD24+ luciferase expressing HCCLM3 cells, tumor of Mouse #1 was developed from 10,000 sorted cells, while tumor of Mouse #2 was developed from 1,000 sorted cells).

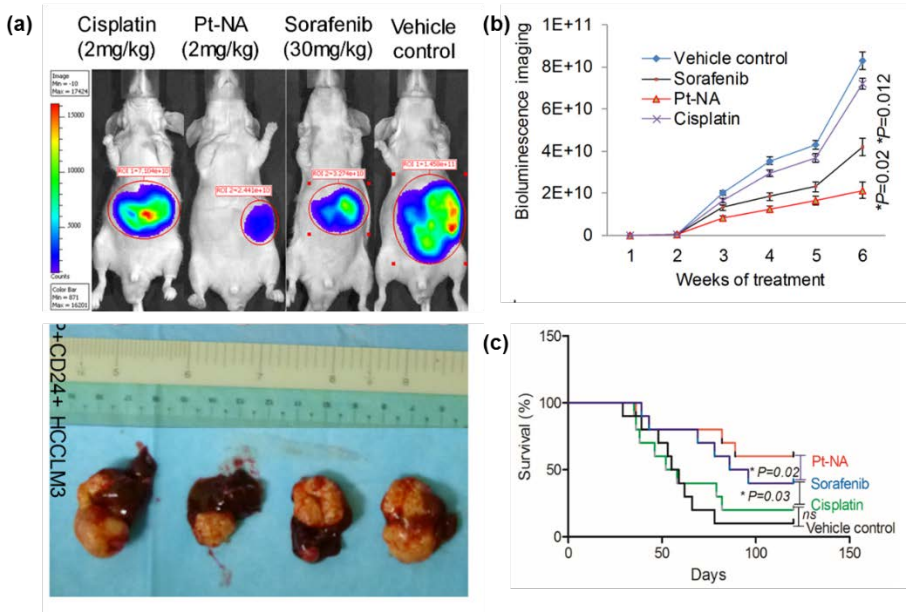

Figure 11. (A) Representative images showing bioluminescence signals and tumor-bearing livers of the orthotopic tumor xenografts at the therapeutic end point of different treatments. (B) Quantitative analysis of bioluminescence signals of all mice in the four treatment groups measured on a weekly basis. (C) The survival analysis of all mice in the four treatment groups.

References

[1] Gottesman, M.; Fojo, T.; Bates, S. *Nat. Rev. Cancer* **2002**, *2*, 48

[2] Maluccio, M.; Covey, A. *Ca-Cancer J. Clin.* **2012**, *62*, 394

[3] European Association For The Study of The Liver. EASL–EORTC clinical practice guidelines: management of hepatocellular carcinoma. *J. Hepatol.* **2012**, *56*, 908

[4] Kim, B. Y. S.; Rutka, J. T.; Chan, W. C. W. *N. Engl. J. Med.* **2010**, *363*, 2434

[5] Mout, R.; Moyano, D. F.; Rana, S.; Rotello, V. M. *Chem. Soc. Rev.* **2012**, *41*, 2539

[6] Farokhzad, O. C.; Langer, R. *ACS Nano* **2009**, *3*, 16

[7] Barry, N. P. E.; Sadler, P. J. *ACS Nano* **2013**, *7*, 5654

[8] Asharani, P. V.; Xinyi, N.; Hande, M. P.; Valiyaveettil, S. *Nanomedicine* **2010**, *5*, 51

[9] Barone, M.; Sciortino, M. T.; Zaccaria, D.; Mazzaglia, A.; Sortino, S. *J. Mater. Chem.* **2008**, *18*, 5531

[10] Chien, C.-T.; Yan, J. Y.; Chiu, W.-C.; Wu, T. H.; Liu, C. Y.; Lin, S. Y. *Adv. Mater.* **2013**, *25*, 5067

[11] Gao, J.; Liang, G.; Zhang, B.; Kuang, Y.; Zhang, X.; Xu, B. *J. Am. Chem. Soc.* **2007**, *129*, 1428

[12] Mironava, T.; Simon, M.; Rafailovich, M. H.; Rigas, B. *Toxicol. In Vitro* **2013**, *27*, 882

[13] Pelka, J.; Gehrke, H. M.; Turk, M.; Crone, M.; Brase, S.; Muller, T.; Blank, H.; Send, W.; Zibat, V.; Brenner, P.; Esselen, M.; Schneider, R.; Gerthsen, D.; Marko, D. *Chem. Res. Toxicol.* **2009**, *22*, 649

[14] Porcel, E.; Liehn, S.; Remita, H.; Usami, N.; Kobayashi, K.; Furusawa, Y.; Le Sech, C.; Lacombe, S. *Nanotechnology* **2010**, *21*, 085103

[15] Shiny, P. J.; Mukherjee, A.; Chandrasekaran, N. *RSC Adv.* **2016**, *6*, 27775

[16] Teow, Y.; Valiyaveettil, S. *Nanoscale* **2010**, *2*, 2607

[17] Xue, X.; Hall, M. D.; Zhang, Q.; Wang, P. C.; Gottesman, M. M.; Liang, X. J. *ACS Nano* **2013**, *7*, 10452

[18] Kim, B. H.; Hackett, M. J.; Park, J.; Hyeon, T. *Chem. Mater.* **2014**, *26*, 59

[19] Sakurai, T.; Shibata, M.; Horiuchi, R.; Yagi, I.; Kondo, T. *Chem. Lett.* **2011**, *40*, 402

[20] Hartmann, J. T.; Lipp, H. P. *Expert Opin. Pharmacother.* **2003**, *4*, 889

[21] Florea, A. M.; Büsselberg, D. *Cancers* **2011**, *3*, 1351

[22] Nie, Z.; Petukhova, A.; Kumacheva, E. *Nat. Nanotechnol.* **2010**, *5*, 15

[23] He, L.; Wang, M.; Ge, J.; Yin, Y. *Acc. Chem. Res.* **2012**, *45*, 1431

[24] Stolarczyk, J. K.; Deak, A.; Brougham, D. F. *Adv. Mater.* **2016**, *28*, 5400

[25] Lee, H.; Sun, E.; Ham, D.; Weissleder, R. *Nat. Med.* **2008**, *14*, 869

[26] Rosi, N. L.; Mirkin, C. A. *Chem. Rev.* **2005**, *105*, 1547

[27] Jin, Y.; Gao, X. *Nat. Nanotechnol.* **2009**, *4*, 571

[28] Pan, Y.; Du, X.; Zhao, F.; Xu, B. *Chem. Soc. Rev.* **2012**, *41*, 2912

[29] Zagorovsky, K.; Chan, W. C. W. *Angew. Chem., Int. Ed.* **2013**, *52*,

3168

[30] Taton, T. A.; Mirkin, C. A.; Letsinger, R. L. *Science* **2000**, *289*, 1757

[31] Ohta, S.; Glancy, D.; Chan, W. C. W. *Science* **2016**, *351*, 841

[32] Li, H.-J.; Du, J.-Z.; Du, X.-J.; Xu, C.-F.; Sun, C.-Y.; Wang, H.-X.; Cao, Z.-T.; Yang, X.-Z.; Zhu, Y.-H.; Nie, S.;Wang, J.. *Proc. Natl. Acad. Sci. U. S. A.* **2016**, *113*, 4164

[33] Sun, Q.; Sun, X.; Ma, X.; Zhou, Z.; Jin, E.; Zhang, B.; Shen, Y.; Van Kirk, E. A.; Murdoch, W. J.; Lott, J. R. *Adv. Mater.* **2014**, *26*, 7615

[34] Ling, D.; Park, W.; Park, S.-j.; Lu, Y.; Kim, K. S.; Hackett, M. J.; Kim, B. H.; Yim, H.; Jeon, Y. S.; Na, K.; Hyeon, T. *J. Am. Chem. Soc.* **2014**, *136*, 5647

[35] Lok, C. N.; Zou, T.; Zhang, J. J.; Lin, W. S.; Che, C. M. *Adv. Mater.* **2014**, *26*, 5550

[36] Fang, J.; Nakamura, H.; Maeda, H. *Adv. Drug Delivery Rev.* **2011**, *63*, 136

[37] Owens, D. E.III; Peppas, N. A. *Int. J. Pharm.* **2006**, *307*, 93

[38] Ashley, C. E.; Carnes, E. C.; Phillips, G. K.; Padilla, D.; Durfee, P. N.; Brown, P. A.; Hanna, T. N.; Liu, J.; Phillips, B.; Carter, M. B. *Nat. Mater.* **2011**, *10*, 389

[39] Wang, Y.; Zhou, K.; Huang, G.; Hensley, C.; Huang, X.; Ma, X.; Zhao, T.; Sumer, B. D.; DeBerardinis, R. J.; Gao, J. *Nat. Mater.* **2013**, *13*, 204

[40] Ling, D.; Hackett, M. J.; Hyeon, T. *Nat. Mater.* **2014**, *13*, 122

[41] Nichols, J. W.; Bae, Y. H. *Nano Today* **2012**, *7*, 606

[42] Ling, D.; Xia, H.; Park, W.; Hackett, M. J.; Song, C.; Na, K.; Hui, K. M.; Hyeon, T. *ACS Nano* **2014**, *8*, 8027

[43] Sambhy, V.; Macbride, M. M.; Peterson, B. R.; Sen, A. *J. Am. Chem. Soc.* **2006**, *128*, 9798

[44] Loher, S.; Schneider, O. D.; Maienfisch, T.; Bokorny, S.; Stark, W. J. *Small* **2008**, *4*, 824

[45] Ashley, C. E. *et al. Nature Mater.* **2011**, *10*, 389

[46] Lo, A., Lin, C.-T. & Wu, H.-C. *Mol. Cancer Ther.* **2008**, ***7***, 579

국문 초록

암 치료 분야의 주요 난제 중 하나는 암의 약물저항성이다. 종양이 기존 화학약물 항암제에 대한 상당한 내성을 갖는 경우 해당 질병에 대한 약물치료의 반응률은 물론 기존에 확립되어 있는 의학적 치료법의 전체적인 효과를 크게 감소시키게 된다.

수 나노미터 단위 크기의 백금 나노클러스터는 항암치료제의 대안 중 하나로 각광받았는데, 이는 클러스터에서 침출되는 백금 이온에서 기인하는 강한 항암효능 때문이다. 하지만 백금 나노클러스터의 비특이적인 투여는 일반 조직에도 독성을 야기할 수 있고 이러한 잠재적인 위험성은 백금 나노클러스터로 하여금 선별적인 종양 표적화 및 백금의 통제된 활성화 및 방출을 가능케 할 수 있는 정교한 전달 체계를 요구하게 한다.

조율된 전달체계를 통해 백금 나노클러스터의 치료 효과의 잠재성을 증진하고 나아가 기존의 약물치료에 대한 한계점을 극복하기 위해 우리는 이번 연구에서 백금 나노클러스터 조립체를 만들었다. 이 조립체는 pH에 대한 반응성과 암세포 표적화 기능이 있는 펩타이드를 작용기로 갖는 고분자 리간드가 백금 나노클러스터를 감싸는 구조이다. 이러한 백금 나노클러스터 조립체

는 순환시 비활성화되었다가 분산되어 있는 암세포 부분모집단을 표적화하여 침투하고 세포 내 낮은 pH 환경에 반응한 조립체 분리를 통해 백금 나노클러스터를 방출함으로써 결국에는 질병세포에 손상을 유도하도록 고안하였다.

잠재적인 암 치료제로서 백금 나노클러스터의 효능을 확인하기 위해 체외 실험 및 생체 내 실험을 진행하였고 기존 백금 기반 항암치료제인 시스플라틴에 대한 약물저항성과 연관되는 간세포암 모델에 백금 나노클러스터를 적용하여 그 효능을 입증하였다.

주요어: 나노클러스터, 기능성 표면 리간드, 자가조립체, 자극반응성, 약물저항성, 약물전달체계, 암치료.

학 번: 2014-22592